communications earth & environment

ARTICLE

https://doi.org/10.1038/s43247-023-00868-5 OPEN

Deglacial perspectives of future sea level for Singapore

Timothy A. Shaw [1✉], Tanghua Li [1], Trina Ng[1,2], Niamh Cahill [3,4], Stephen Chua [1], Jedrzej M. Majewski [1], Yudhishthra Nathan [1], Gregory G. Garner[5], Robert E. Kopp [6,7], Till J. J. Hanebuth [8], Adam D. Switzer [1,9] & Benjamin P. Horton [1,9]

Low elevation equatorial and tropical coastal regions are highly vulnerable to sea level rise. Here we provide probability perspectives of future sea level for Singapore using regional geological reconstructions and instrumental records since the last glacial maximum ~21.5 thousand years ago. We quantify magnitudes and rates of sea-level change showing deglacial sea level rose from ~121 m below present level and increased at averaged rates up to ~15 mm/yr, which reduced the paleogeographic landscape by ~2.3 million km^2. Projections under a moderate emissions scenario show sea level rising 0.95 m at a rate of 7.3 mm/yr by 2150 which has only been exceeded (at least 99% probability) during rapid ice mass loss events ~14.5 and ~9 thousand years ago. Projections under a high emissions scenario incorporating *low confidence* ice-sheet processes, however, have no precedent during the last deglaciation.

[1] Earth Observatory of Singapore, Nanyang Technological University, Singapore, Singapore. [2] Centre for Climate Research Singapore, Singapore, Singapore. [3] Department of Mathematics and Statistics, Maynooth University, Maynooth, Ireland. [4] Irish Climate Analysis and Research UnitS (ICARUS), Maynooth University, Kildare, Ireland. [5] Gro Intelligence, New York, NY, USA. [6] Department of Earth & Planetary Sciences, Rutgers University, New Brunswick, NJ, USA. [7] Institute of Earth, Ocean & Atmospheric Sciences, Rutgers University, New Brunswick, NJ, USA. [8] Department of Marine Science, Coastal Carolina University, Conway, SC, USA. [9] Asian School of the Environment, Nanyang Technological University, Singapore, Singapore. ✉email: tshaw@ntu.edu.sg

Over the 21st century, continuing relative sea level (RSL) rise poses an existential threat to low-lying islands, coastal deltas and lowlands and their respective environments and populations[1–5]. The implications of rising sea level, however, will be spatially disproportionate with equatorial and tropical latitudes of Asia facing the greatest impacts where substantial populations live below projected sea- and flood-levels[1,6,7]. Singapore, a small (~730 km^2) equatorial island sustaining ~5.9 million people in Southeast Asia (Fig. 1), is highly exposed to sea-level rise with centres of population, industry, urban, and transport infrastructure within 2 m elevation of present sea level[8,9]. Accurate sea-level projections are required to implement appropriate adaptation, mitigation, and engineering strategies[8,10].

A prerequisite for sea-level projections is understanding the relationship between changes in the climate and changes in sea level[11–13]. Most instrumental sea-level records, however, are temporally limited to the mid-to-late twentieth and early twenty-first centuries[14,15] and capture a sea-level/climate relationship during which anthropogenic forcing dominates[4,16,17]. This is especially true in Singapore, where near-complete instrumental records only began in the early 1970s (Fig. 2; Table 1). Reconstructions of RSL change based on geological proxies can provide complementary archives, demonstrating the longer-term response of sea level over centuries to millennia to a wider range of climate forcing mechanisms, unforced climate variability, and boundary conditions[12,18–21]. Both geological reconstructions and instrumental records, however, share fundamental challenges in understanding spatial and temporal variability driven by processes that cause regional sea level to deviate from the global mean[11,13,22,23].

Geological reconstructions from equatorial and tropical latitudes have provided detailed RSL histories since the last glacial maximum (LGM) ~ 26 thousand years (kyr) to ~19 kyr before present (BP)[24–27]. These reconstructions have been central to our understanding of global mean sea level (GMSL), determine ice-volume changes and constrain geophysical models of the glacial isostatic adjustment (GIA) process[19,28]. Understanding the timing, magnitude and driving processes of past RSL changes provides a useful background to contextualise sea-level projections[12] that is important in the context of effective coastal risk management strategies for emerging contingencies[5,29].

Here we present a synthesis of the evolution of RSL in equatorial Southeast Asia combining geological reconstructions and instrumental records of RSL change from the Sunda Shelf and Singapore. This region is important because of the availability of detailed RSL datasets spanning the LGM (~21.5 kyr BP) through the last deglacial transition (LDT, ~18–11 kyr BP)[26,30], Holocene (~11 kyr BP)[31] and present instrumental period (20th and 21st century)[15,32] that are not unduly affected by vertical land motion processes[33–35]. We apply an Error-In-Variables Integrated Gaussian Process (EIV-IGP) model[36] to quantify magnitudes and rates of RSL change through time and assess and discuss paleogeographic changes across the Sunda Shelf in response to RSL change using a GIA model[37,38]. We conclude with the latest Intergovernmental Panel on Climate Change (IPCC) sea-level rise projections to 2150 for Singapore[4,39] and use the geological past to quantitatively provide probability perspectives when projected rates of sea level were last exceeded. We show that projected rates of RSL rise under a moderate emission scenario were only last exceeded (at least 99% probability) during rapid ice mass loss events of the last deglacial period.

Results and discussion

Last glacial maximum to present relative sea-level changes. The geological RSL reconstructions from the former North Sunda River on the central Sunda Shelf (Fig. 1a) provide a sea-level index point (SLIP) dataset ($n = 33$) that constrain RSL between ~21.5 kyr and ~13.3 kyr BP with an average vertical and age uncertainty of ±5 m (2σ) and ±393 years (2σ), respectively (Fig. 3a). The vertical uncertainty incorporates spatial differences in GIA between the Sunda Shelf and Singapore. Application of the EIV-IGP model shows RSL rose from a lowstand of −121.1 m at 20.7 kyr BP to −112.3 m at ~19 kyr BP at rates of RSL rise up to 7 ± 5.8 mm/yr

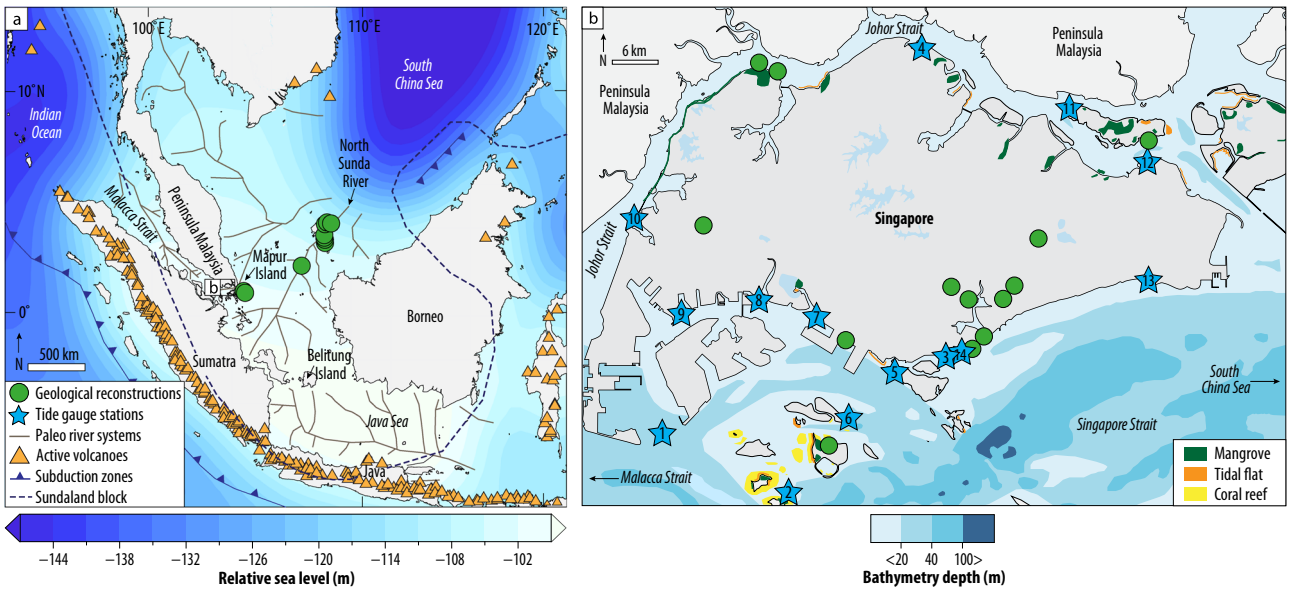

Fig. 1 Southeast Asia study region and location of relative sea level (RSL) datasets. a RSL predictions at the last glacial maximum 26 thousand years before present from glacial isostatic adjustment model consisting of the ICE-6G_C ice model[37,38] and HetM-LHL140 3D Earth model[124,125]. Location of paleo river systems[113,115] and geological RSL reconstructions from the Sunda Shelf[26,30] and Mapur Island, Indonesia[32]. **b** Singapore study area showing location of geological RSL reconstructions[31] and tide gauge stations[15] shown in Fig. 2 and detailed in Table 1. Present-day simplified bathymetry depth and approximate distribution of coastal habitats adapted after refs. [92] and [102], respectively. Black dashed line in panel a indicates the approximate boundary of the Sundaland block and the dark blue barbed line indicates the location of major subduction zones (after ref. [35]). Location of active and potentially active volcanoes after ref. [120]. Numbering of tide gauge stations in panel b and associated names are provided in Table 1.

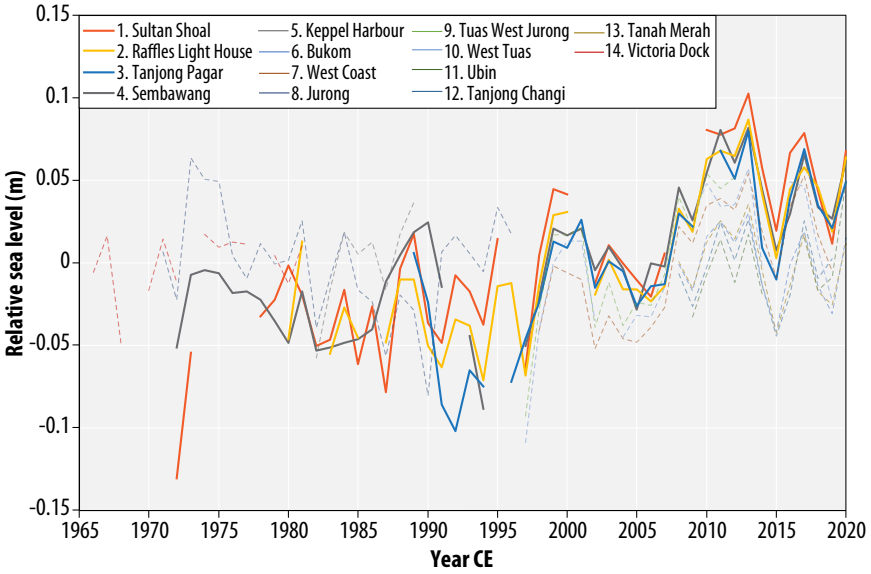

Fig. 2 Singapore tide gauge records. Annual relative sea level (RSL) change recorded by Singapore tide gauge stations[15] shown in Fig. 1b and detailed in Table 1. Thicker lines (stations 1–4) represent tide gauge stations used to construct an averaged instrumental RSL record discussed in text.

Table 1 Summary of Singapore tide gauge stations.

Figure 1b map #	PSMSL ID	Station name	Time span of data	Completeness of record (%)
1	1248	Sultan Shoal*	1969–2020	91
2	1351	Raffles Lighthouse*	1973–2020	88
3	1746	Tanjong Pagar*	1989–2020	98
4	724	Sembawang*	1954–2020	83
5	1534	Keppel Harbour	1981–1989	93
6	2032	Bukom	2008–2020	100
7	1895	West Coast	1997–2019	99
8	1275	Jurong	1970–1997	95
9	1894	Tuas West Jurong	1997–2013	98
10	1896	West Tuas	1997–2019	90
11	2068	Ubin	2009–2020	92
12	2033	Tanjong Changi	2008–2020	100
13	2034	Tanah Merah	2008–2020	100
14	1183	Victoria Dock	1966–1981	92

PSMSL permanent service for mean sea level. *=tide gauge stations used to construct an averaged record for Singapore described in text.
Metadata of Singapore tide gauge stations from which instrumental measurements of 20th and 21st century relative sea level change were extracted[15].

(Fig. 3d, e). The rate of RSL subsequently slowed to an average ~3 mm/yr as RSL continued rising to −105.2 m at ~16 kyr BP. Between ~16 kyr and ~13 kyr BP, RSL rose to −~70 m with a cluster of SLIPs ($n = 17$) between ~15 kyr and ~14 kyr BP associated with the meltwater pulse 1A (MWP1A) event (Fig. 3d). The average (250-time interval) rate of RSL rise between 16 kyr and 13 kyr BP reached 15.4 ± 8.2 mm/yr (Fig. 3e). An absence of SLIP data constraining the LDT into the early Holocene is reflected by the increased uncertainty of RSL changes during this period.

The geological RSL reconstructions from mainland Singapore and neighbouring islands (Fig. 1b) provide a SLIP dataset ($n = 64$) that constrain RSL between ~9.4 kyr and ~1.2 kyr BP with an average vertical and age uncertainty of ±1.1 m and ±487 years, respectively (Fig. 3b). Most SLIPs (n = 59) are concentrated towards the early- to mid-Holocene and shows a continuous rise in RSL. The EIV-IGP model shows RSL rose from −20.6 m at 9.4 kyr BP to −0.25 m at ~7 kyr BP (Fig. 3d) at a maximum rate of 15.2 ± 3.5 mm/yr (Fig. 3e). The rate of RSL rise subsequently slowed as RSL continued to rise and reached a mid-Holocene highstand of ~4.6 m at 5.2 kyr BP. SLIPs constraining the mid- to late-Holocene transition are sparse ($n = 4$) but suggest RSL fell below present level to −2.2 m between ~2.5 kyr and ~0.25 kyr BP at a rate of −1 mm/yr.

The geological RSL reconstructions from Mapur Island, Indonesia (Fig. 1a) provide a SLIP dataset ($n = 16$) that constrain RSL between 1915 and 2012 CE with an average vertical and age uncertainty of ±0.1 m and ±1.4 years, respectively (Fig. 3c). The averaged tide gauge record for Singapore provides annual instrumental measurements of RSL change between 1972 and 2020 CE (Fig. 3c). The EIV-IGP model applied to the combined dataset shows RSL rose 0.15 m between 1915 and 2020 CE (Fig. 3d) at rates of RSL rise increasing from 1.7 ± 1 mm/yr to 2.2 ± 0.6 mm/yr (Fig. 3e).

Paleogeographic changes. Rising RSL dramatically altered the paleogeographic landscape of Southeast Asia (Fig. 4a). At the LGM, the area of the land exposed on the Sunda Shelf was greater (relative to present-day topography) by ~2.3 million km^2 (Fig. 4b). During the LDT, RSL rise flooded the Sunda Shelf at an

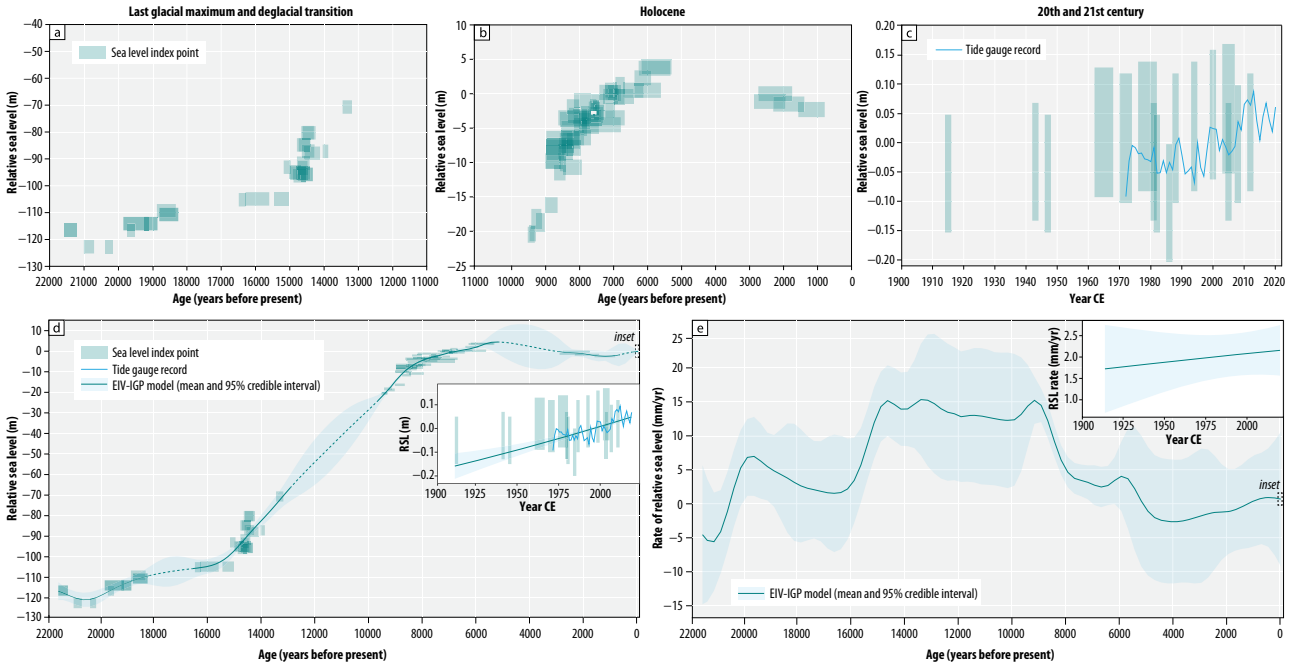

Fig. 3 Geological reconstructions and instrumental records of relative sea level (RSL) change from the Sunda Shelf and Singapore. Sea level index points (SLIPs) showing RSL change since (**a**) the last glacial maximum and deglacial transition[26,30], **b** Holocene[31], and **c** 20th and 21st century[15,32] (note axis change among graphs). Application of the Error-in-Variables Integrated Gaussian Process (EIV-IGP) model[36] to a combined sea-level dataset showing (mean and 95% credible interval) **d** magnitudes and **e** rates of RSL change. Inset panels shows magnitudes and rates of RSL change for the combined geological and averaged instrumental dataset for the 20th and 21st century. EIV-IGP model mean dashed line in (**d**) represents time periods with an absence of SLIPs and increasing RSL change uncertainty.

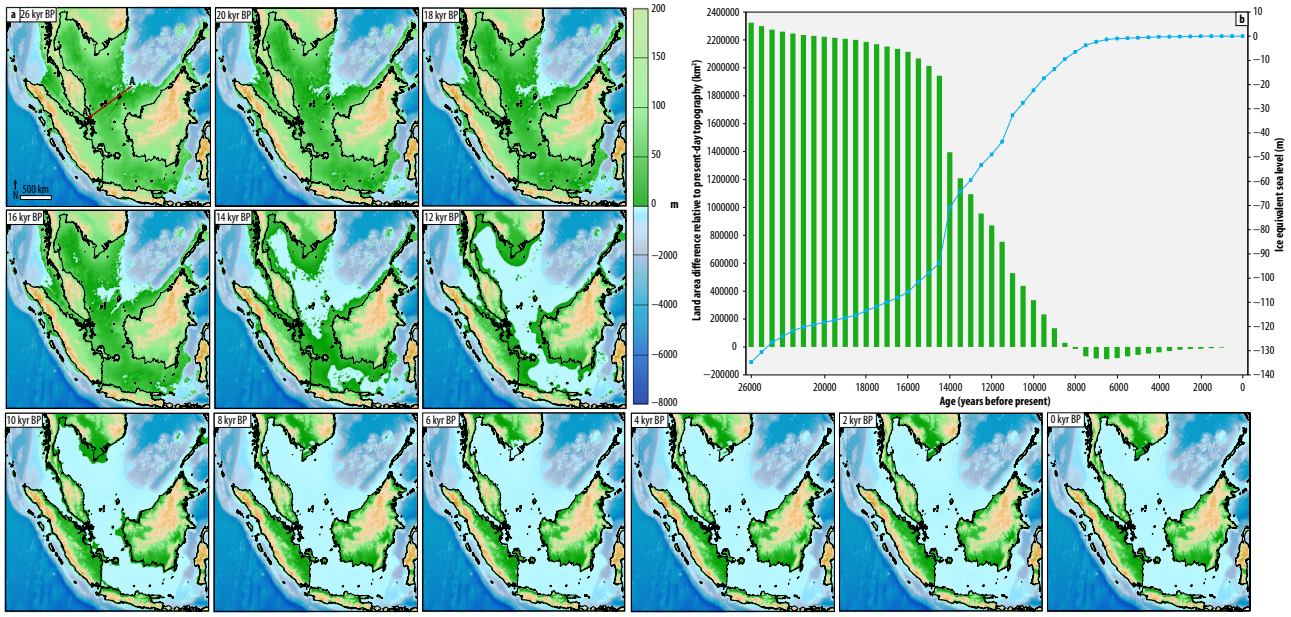

Fig. 4 Land area change since the last glacial maximum (LGM). a Paleotopographic maps showing land area change as rising sea level flooded the Sunda Shelf after the LGM 26 thousand years (kyr) before present (BP) to 20 kyr BP and then at 2 kyr intervals thereafter. **b** Calculated land area difference relative with present-day topography[132] and ice equivalent sea level from 26 kyr BP based on the ICE-6G_C global ice history model[37,38]. Paleogeographic changes continued as ice equivalent sea level ceased during the mid-Holocene because of spatially variable GIA processes as discussed in text. Red transect line A-A′ in 26 kyr BP panel used to calculate lateral transgression rates discussed in text.

average lateral shoreline migration rate of 57 m/yr and by 16 kyr BP, exposed land area had reduced to ~2.1 million km^2. The rapid increase in RSL rise during MWP1A reduced land area to ~1.4 million km^2 and lateral shoreline migration rates increased to ~335 m/yr. By the early Holocene (~10 kyr BP), land bridges between continental and insular islands of Southeast Asia such as Sumatra and Borneo had been severed and exposed land area was further reduced to ~336 ka km^2 at a maximum rate of ~15 m/yr. During the mid-Holocene (~6 kyr BP), rising RSL reaching above present level decreased exposed land area to a minimum of

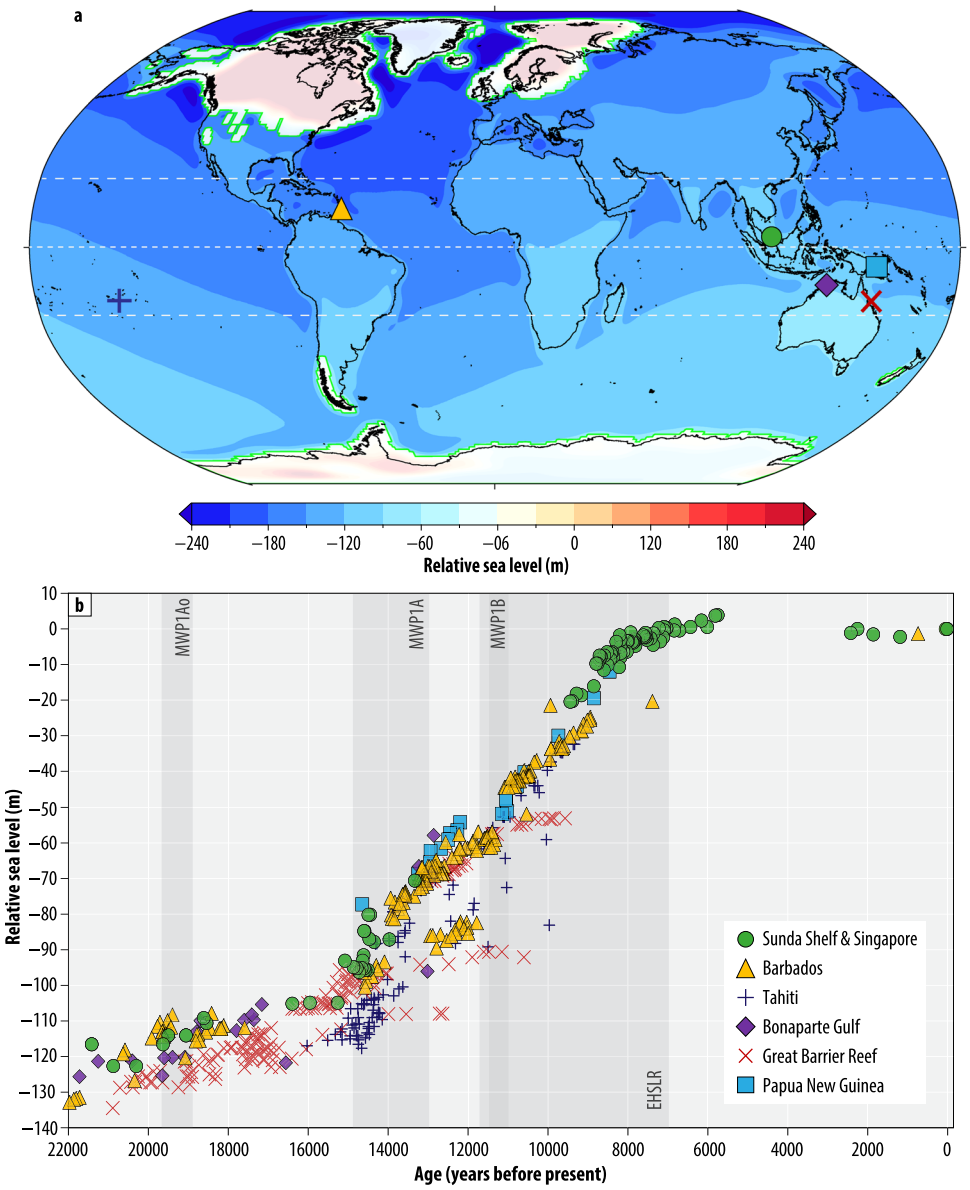

Fig. 5 Geological relative sea level (RSL) reconstructions since the last glacial maximum (LGM) from equatorial and tropical latitudes. a Global map showing RSL predictions at 26 thousand years (kyr) before present (BP) from glacial isostatic adjustment model consisting of the ICE-6G_C ice model[37,38] and HetM-LHL140 3D Earth model[124,125]. Location of geological reconstructions constraining RSL changes since the LGM within equatorial and tropical latitudes (white dashed lines). **b** Geological reconstructions of RSL change from sites in (**a**) since 22 kyr BP including the Sunda Shelf and Singapore (green circles, this study), Barbados (yellow triangles[28,54]), Tahiti (dark blue cross-hairs[25,49]), Bonapate Gulf (purple diamonds[27]), Great Barrier Reef (red crosses, Hydrographer's Passage[134]) and Papua New Guinea (light blue squares[135,136]). Each geological reconstruction are derived using sea-level indicators (e.g., coral reefs and mangroves) that are chronologically constrained using a variety of dating techniques (e.g., U-Th and C14 dating). The reader should see original publications for discussions on their associated vertical and temporal uncertainties, respectively. No additional corrections for local vertical land motion have been applied to the geological reconstructions and the reader should see original publications for discussions on their regional setting. Bright green outline with white shading in panel a represents spatial extent of ice sheets at the LGM. Dark grey vertical shading in (**b**) represents approximate global timing and name of late Quaternary rapid increases in global mean sea level discussed in text[47,70]. MWP meltwater Pulse, EHSLR early Holocene sea level rise.

-88 ka km^2 before subsequently increasing again thereafter as RSL fell towards present reaching a near present-day coastline configuration by ~2–1 kyr BP.

Last glacial maximum and deglacial transition. Geological reconstructions from the Sunda Shelf and Singapore reveal the response of sea level to climate forcing as the Earth transitioned from glacial to interglacial conditions. Between ~26 kyr and ~19 kyr BP, global ice sheet complexes grew to their maximal extent[19,27,40] and GMSL reached a lowstand of ~120 to ~130 m below present level (Fig. 5a, b). Atmospheric CO_2 concentrations were between ~188 and ~194 ppm and global mean surface temperature (GMST) cooler (relative to 1850–1900 CE) by 5°–7°C[41,42].

Increasing northern summer insolation began the onset of the LDT towards the early Holocene[12,43] as atmospheric CO_2 concentrations increased to ~270 ppm and GMST rose 1°–1.5 °C kyr[42]. In response, GMSL rose as ~50 million km^3

land-based ice was transferred to the global ocean primarily from deglaciating Northern Hemisphere ice masses[27,40,44,45]. This ice melt caused RSL on the Sunda Shelf to rise ~93 m over ~12,000 years from 21.5 kyr to 9.5 kyr BP at an average rate of ~7.6 mm/yr.

Superimposed on long-term secular rising GMSL have been several periods of short-term rapid increases[46,47]. An initial rapid increase in GMSL between 19.5 kyr and 18.8 kyr BP (MWP1Ao, Fig. 5b) caused RSL on the Sunda Shelf to rise ~8 m at rates of RSL rise up to 7 mm/yr (Fig. 3d, e). Similar rapid increases in RSL following termination of the LGM have been reported from geological reconstructions in both low[27] (Fig. 5a, b) and high[48] latitude settings.

A second rapid increase in GMSL between 14.8 kyr and 13 kyr BP (MWP1A, Fig. 5b) caused RSL on the Sunda Shelf to rise ~32 m at rates of RSL rise up to ~15 mm/yr (Fig. 3d, e). This averaged rate is conservative compared to annual rates of RSL rise of ~40 mm/yr[26,47,49]. Rising GMSL during MWP1A was the most rapid of the last deglacial period and was driven by the sudden influx of meltwater as deglaciation of Northern Hemisphere ice sheets continued and ice-dammed and subglacial lakes drained increasing ocean volume by ~470,000 km^3 [19,47,50,51]. Geological reconstructions to support MWP1A are global in scale with widespread evidence within equatorial and tropical latitudes (Fig. 5 and references therein) that are also corroborated at higher latitudes[52,53].

An additional rapid increase in GMSL during the LDT is postulated between ~11.5 kyr and ~11 kyr BP (MWP1B, Fig. 5b). Evidence from coral reconstructions in Barbados suggests RSL rose ~13 m at rates of RSL rise increasing ~20–40 mm/yr[24,25,54] while Gargani[55] reported rates of RSL rise may have been even faster at ~65 mm/yr. The global importance of MWP1B, however, remains contested[19] and is currently unresolved in other equatorial and tropical reconstructions with an equivalent change in RSL not recorded on the Sunda Shelf and Tahiti[26,49]. Indeed ref. [19] suggests elevated rates of RSL increasing at ~16.5 mm/yr occurred just prior to MWP1B between 12.5 ka and 11.5 ka BP after the Younger Dryas. While mangrove and intertidal data ($n = 5$) from the Southern Vietnam Shelf provide evidence of RSL change between ~-65 m and ~-50 m between ~13 kyr and ~11 kyr BP[26] (Supplementary Fig. 1), they were not included here due to their spatial distance from North Sunda River and Singapore SLIP datasets and their proximal location to the Mekong River Delta and its associated influence of subsidence[19,56].

The rise in GMSL after the LGM had profound impacts on shelf margins[57] including the Sunda Shelf and transformed the palaeogeography of the region[58–60]. The low shelf gradient allowed sea level to rapdily transgress laterally increasing from an average rate of ~57 m/yr to ~335 m/yr during MWP1A. Rising RSL submerged coastal landscapes[60,61] and segregated insular islands of Southeast Asia from the continental mainland dislocating flora and fauna migration routes[59,62]. Indeed, evidence from whole-genome sequencing datasets suggests rising RSL, particularly during MWP1A, played an important role in the spatial distrbution of modern human demography in Asia as local populations became segregated[63]. In the Singapore Strait, the land bridge that existed during low GMSL was severed as rising seas flooded across sills to the east from the South China Sea and to the west from the Malacca Strait when RSL reached ~−30 m toward the end of the LDT[64] (Fig. 1b). The flooding of the Sunda Shelf also altered the interchange of water between the Indian Ocean and South China Sea distrupting regional oceanographic and atmospheric climate systems[65–67].

Holocene. Climate forcing during the Holocene up until the pre-industrial Common Era (~1850 CE) was relatively mild compared to the preceding LDT. Atmospheric CO_2 concentrations were between ~260 and ~285 ppm[42] and variability in GMST was reduced[68] showing a slight but steadily warming trend of ~0.25–0.5 °C[41,69]. Despite relative climate stability, GMSL continued to rise tens of metres during the early Holocene as Northern Hemisphere ice sheets entered their final stages of disintegration and coastal ice streams broke[19,70–72].

In Singapore, RSL rose ~21 m between 9.5 kyr and 7 kyr BP at rates of RSL rise up to ~15 mm/yr (Fig. 3d, e). Bird et al.[73,74] suggested rapid RSL rise during the early Holocene in Singapore was temporally punctuated by a near cessation in RSL rate between 7.8 kyr and 7.4 kyr BP before continuing to rapidly increase again thereafter. Lambeck et al.[19], however, noted that the near-zero RSL rise during this period possibly reflects local processes because of an absence of similar trends at the global scale. Furthermore, Chua et al.[31] concluded accurate verification of oscillating RSL in Singapore is precluded by large vertical and temporal scatter of SLIP data following their standardisation[75].

Rising RSL reached near present level by ~7 kyr BP and continued rising to a mid-Holocene highstand that is characteristic of far-field regions distal from ice sheets and driven by regional hydro-isostatic processes when meltwater input decreased[21,22]. The magnitude and timing of the highstand varies around the Sunda Shelf[31,76,77] and in Singapore, RSL reached ~4.6 m at ~5 kyr BP. Falling RSL from the mid-Holocene highstand was driven by both hydro- and glacio-isostatic loading of the Earth's surface (equatorial ocean syphoning and continental levering)[78] and rotational feedback[79]. Late-Holocene SLIPs show RSL below present at −~2 m between ~2.5 kyr and ~0.5 kyr BP. Evidence to support RSL below present during the late Holocene is corroborated by mangrove SLIPs from Peninsula Malaysia which show RSL at ~−0.7 m ~ 0.8 kyr BP[33,80–82].

The rise and fall in RSL during the Holocene continued to alter the palaeogeography of the region. Rapid RSL rise during the early Holocene flooded lowlands surrounding Singapore and in the Johor Strait segregating Singapore from Peninsula Malaysia[64,83]. As the rate of RSL rise declined below ~7 mm/yr after ~8.5 kyr BP, widespread development of mangrove forests commenced as mangroves began to maintain their vertical position through sediment accretion[84]. The rise in RSL above present during the mid-Holocene continued to encroach and submerge low elevations of Singapore decreasing the terrestrial land area. The marine sediments that were deposited were subsequently weathered and partially eroded by sub-aerial processes as RSL fell during the late Holocene increasing land area as previous shorelines became progressively exposed[85].

Twentieth and twenty-first century. Instrumental records cover changes in Earth's climate driven by anthropogenic forcing[86]. Atmospheric CO_2 concentrations have increased to ~424 ppm in 2023 CE[87], which is unprecedented in at least the last two million years, and GMST rose ~1.1 °C between 1850–1900 and 2011–2020, which is warmer than any multi-centennial interval during the LDT[42]. The response of GMSL to this forcing has so far been an increase in rate from ~1.4 mm/yr[4,88–90] between 1901 and 1990 to 3.3 mm/yr between 1993 and 2018 that was driven by accelerating land-ice losses and thermal expansion that vary in relative contribution depending on time period analysed[4]. For example, sea-level budgets for the 20th and 21st century reveal thermal expansion accounted for 32% of GMSL rise between 1901 and 1990 compared to 46% between 1993 and 2018[4]. Long-term (i.e. >50 years) instrumental records coupled with overlapping geological reconstructions have also demonstrated rising GMSL during the 20th century was faster ($P \geq 0.999$) than the proceeding 3 kyr[17], with a timing of emergence above background

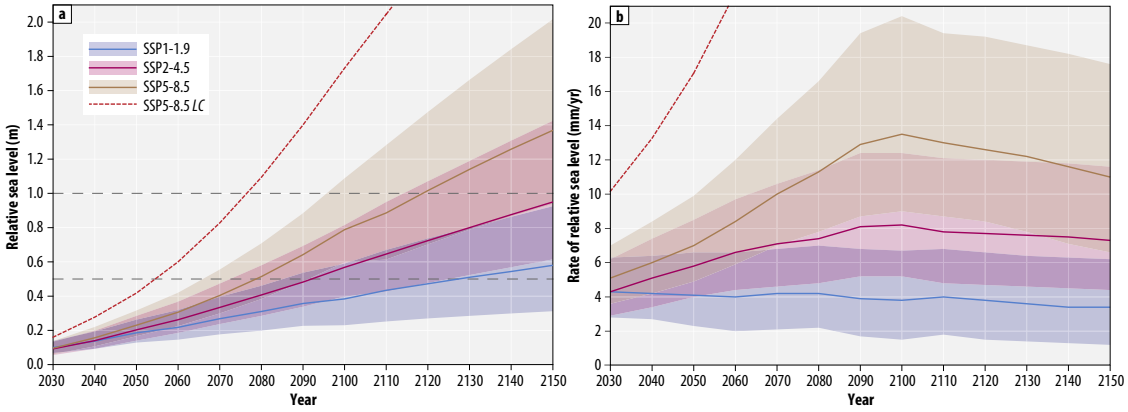

Fig. 6 Future projections of relative sea-level (RSL) rise to 2150 for Singapore. a Magnitudes and **b** rates of RSL rise to 2150 for Singapore showing 50th percentile (solid line) and likely (17th–83rd percentile; shading) ranges for Shared Socioeconomic Pathways (SSP) 1-1.9, SSP2-4.5 and SSP5-8.5 scenarios. Red dashed line represents the 83rd percentile projection for SSP5-8.5 *low confidence* (*LC*) scenario. See Supplementary Table 1 for full decadal values to 2150. Projections are relative to 1995–2014 baseline period for the Sultan Shoal tide gauge station[4,39] (Fig. 1b). Grey horizontal dashed lines in panel a used to reflect timing of exceedance of 0.5 m and 1.0 m magnitude thresholds discussed in text.

variability centred on 1863 CE[91]. In Southeast Asia, geological reconstructions using mangrove sediments from Peninsula Malaysia have suggested an increase in RSL rate from 1.26 mm/yr to 3.2 mm/yr after 1900 CE[80].

The addition of geological reconstructions from Mapur Island, Indonesia provides an important methodological step toward further extending instrumental records of RSL change in equatorial and tropical latitudes such as Singapore[32]. The combined dataset shows RSL rose 0.15 m between 1915 and 2020 CE increasing from a rate of ~1.7 mm/yr to ~2.2 mm/yr. Singapore's temporally limited instrumental records provide only a brief history of RSL changes with variability on different timescales[92–94]. On daily to seasonal timescales, sea-level variability is influenced by meteorological forcing across the region[95] and prevailing wind directions during Northern Hemisphere and Southern Hemisphere monsoon systems can cause sea level to vary up to ±30 cm[92]. Indeed, storm surges driven by winds over the South China sea can result in localised coastal flooding when coinciding with high spring tides[96]. On inter-annual timescales, sea-level variability is dominated by the El Niño–Southern Oscillation and during El Niño and La Niña events, changes in sea-surface height can vary by up to ±5 cm, with lower sea-surface height observed during El Niño events[92]. On decadal and inter-decadal timescales, sea-level variability in Singapore and wider Southeast Asia is influenced by basin-scale climate modes including the Pacific Decadal Oscillation and Interdecadal Pacific Oscillation[97,98].

Coastal landscape changes following British colonial establishment in 1819 and during the 20th and 21st century in Singapore largely reflect anthropogenic modifications to accommodate industrial and urban development[99]. Land reclamation projects expanded land area ~25% from 581.5 km^2 in 1960 to 733.2 km^2 in 2022[99] that significantly reduced coastal habitat extent[100–102]. Between 1922 and 2011, tidal flats and coral reefs reduced in area from 33 km^2 to 5 km^2 and 32 km^2 to 9.5 km^2, respectively. Furthermore, the damming of mangrove-fringed estuaries to create freshwater reservoirs resulted in a 91% decrease in mangrove forest extent, reducing in area from 75 km^2 to 6.4 km^2 [101,102].

Perspectives of future sea level. The magnitude RSL rise since the end of LGM through the LDT, Holocene and towards the present demonstrates the long-term commitment and sensitivity of sea levels to climate forcing on timescales of centuries to millennia[12]. While the extent and grounding line of ice sheets were spatially different at the LGM compared to present conditions[4,103] (Fig. 5a), it is virtually certain (at least 99% probability) Greenland and likely (at least 66% probability) Antarctic ice sheets will continue losing mass throughout the 21st century[4]. Indeed, rising GMSL initiated during the 20th century is virtually certain to continue even if CO_2 emissions are drastically reduced due to the lagging integrated response time of deep ocean heat uptake and ice sheets[12,104–107]. Over the next 2000 years, GMSL is committed to rise 2–3 m if GMST is limited to 1.5 °C warming, 2–6 m if limited to 2 °C warming and 19–22 m with 5°C of warming[4]. Projections of GMSL rise are consistent with geological reconstructions during past warm climate periods when GMST were higher[108]. For example, during the last interglacial ~126 kyr to 116 kyr BP, GMSL was ~1–5 m higher than present when GMST were just 0.5–1 °C warmer than today[4,108–110].

Future sea-level rise in Singapore will primarily be caused by global increases in ocean mass and volume associated with meltwater input from land-based ice sheets and glaciers and thermal expansion to warming temperatures[4]. Faster-than-projected disintegration of marine ice shelves may also exacerbate sea-level rise through marine ice cliff instability processes[111,112] for which there is *low confidence*[4]. In contrast, the impact of vertical land motion processes will be negligible due to the tectonic stability and overall low subsidence rates throughout the central Sunda Shelf including Singapore[33,34,64].

Under the very low emissions shared socioeconomic pathway (SSP)1–1.9 scenario, future RSL rise (relative to a 1995–2014 baseline) in Singapore will increase 0.58 m (likely range of 0.31–0.93 m) at a rate of 3.4 mm/yr (1.2–6.2 mm/yr) by 2150 (Fig. 6a, b, Supplementary Table 1). Magnitude 0.5 m and 1.0 m thresholds under SSP1–1.9 are expected to be surpassed by 2127 (likely range of 2084–>2300) and 2279 (2162–>2300), respectively. The geological past provides probability perspectives to when equivalent rates of RSL rise were last exceeded (Fig. 7). Rates of RSL rise increasing at greater than 3.4 mm/yr were very likely (at least 90% probability) between ~20 kyr and ~19.5 kyr BP and about as likely as not (between 33 and 66% probability) between 18.75 kyr and 16 kyr BP (Fig. 7a). Rates of RSL rise exceeding 3.4 mm/yr were virtually certain to have occurred between 15.25 kyr and 13.5 kyr BP and between 9.5 kyr and 8.25 kyr BP. During the last ~5 kyr, it is unlikely (less than 33% probability) rates of RSL rise exceeded 3.4 mm/yr.

Under the moderate emissions SSP2-4.5 scenario, future RSL in Singapore will increase 0.95 m (0.62–1.4 m) at a rate of 7.3 mm/yr

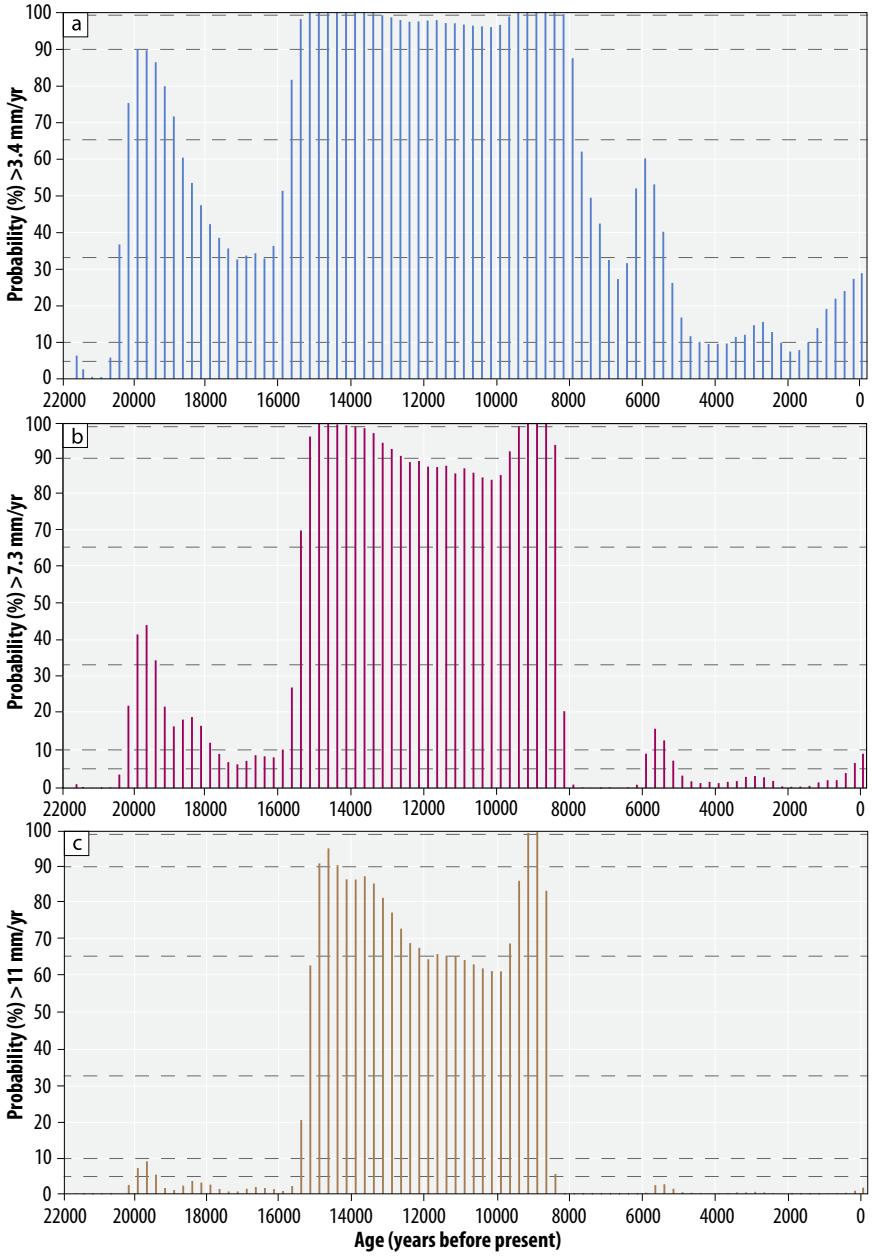

Fig. 7 Geological probability perspectives of future relative sea-level (RSL) rise. Probability (%) of rates of RSL rise during the geological past based on 250-year average bins exceeding **a** 3.4 mm/yr, **b** 7.3 mm/yr and **c** 11 mm/yr that reflect projected (50th percentile) rates of RSL rise by 2150 under SSP1-1.9, SSP2-4.5 and SSP5-8.5 scenarios, respectively. Grey horizontal dashed lines indicate likelihood ranges discussed in text.

(4.4–11.6 mm/yr) by 2150 (Fig. 6a, b, Supplementary Table 1). Magnitude 0.5 m and 1.0 m thresholds under SSP2-4.5 are expected to be surpassed by 2092 (2072–2125) and 2157 (2114–2264), respectively. Rates of RSL rise exceeding 7.3 mm/yr were about as likely as not between ~20 kyr and ~19.5 kyr BP and unlikely up to 15.75 kyr BP (Fig. 7b). Rates of RSL rise exceeding 7.3 mm/yr were virtually certain between 15 kyr and 14 kyr BP and between 9.25 kyr and 8.75 kyr BP. During the last ~8 kyr, it is unlikely rates of RSL rise exceeded 7.3 mm/yr.

Under the very high emissions SSP5-8.5 scenario, future RSL rise in Singapore will increase 1.37 m (0.94–2.02 m) at a rate of 11 mm/yr (6.6–17.6 mm/yr) by 2150 (Fig. 6a, b, Supplementary Table 1). Magnitude 0.5 m and 1.0 m thresholds under SSP5-8.5 are expected to be surpassed by 2080 (2066–2097) and 2119 (2096–2159), respectively. Rates of RSL rise exceeding 11 mm/yr were very unlikely (less than 10% probability) between 21.5 kyr and 15.75 kyr BP while it very likely occurred between 15.25 kyr and 14.75 kyr BP and virtually certain at ~9 kyr BP (Fig. 7c). During the last ~8.25 kyr, it is extremely unlikely (less than 5% probability) rates of RSL rise exceeded 11 mm/yr.

Considering ice-sheet processes in which there is currently *low confidence* in the scientific ability to model raises the potential sea-level rise contributions, particularly under high emissions scenarios. The 83rd percentile projection for SSP5-8.5 including *low confidence* marine ice cliff instability processes reaches 5.3 m and 111 mm/yr by 2150 (Supplementary Table 1) and moves the crossing of a 1.0 m magnitude threshold as soon as 2076 (Fig. 6a). Such high rates of RSL rise have no precedent in the last ~21.5 kyr.

The geological past also provides useful perspectives to future topographic changes. While present and future coastal configurations are anthropogenically modified and future RSL rise will

be spatially variable across Southeast Asia, a projected rise of 0.95 m by 2150 under SSP2-4.5 (Supplementary Table 1), for example, caused an equivalent reduction in the paleogeographic landscape of −19.7 ka km^2 during the mid-Holocene. A projected RSL rise of ~5 m by ~2150 under the high emissions *low confidence* scenario (Supplementary Table 1) caused the paleogeographic landscape to reduce −87.6 ka km^2 during the mid-Holocene (Fig. 4b) and illustrates the vulnerability of equatorial and tropical coastal regions and population densities to future RSL rise[1].

Methods

Regional setting and sea-level datasets. Singapore is located at the centre of the Sunda Shelf, the largest tropical shelf margin in the world, which extends ~800 km laterally over low geomorphic gradients towards the deep-ocean South China Sea (Fig. 1). During glacial periods of low sea level, present-day islands of Borneo, Java, Sumatra, and Singapore were connected with continental Asia[59,60]. This subaerially exposed land mass, known as Sundaland[113,114], was dissected by several major river systems that drained the surrounding exposed shelf and its hinterland[113,115] (Fig. 1a) and have preserved deposits pertaining to the paleoenvironmental evolution of the region[58–60,115,116]. Plate tectonic movements and the northward moving Indo-Australian Plate colliding with the Eurasian Plate[117,118] causes major seismicity from tectonics and volcanism to be concentrated towards plate exterior subduction and collision zones[35,119,120] (Fig. 1a). The interior of Sundaland, however, is virtually free of seismicity and volcanic activity[35,119,120] and vertical deformation is considered minimal during the Quaternary[33,121]. Decade long GPS velocities support this inference showing a very low rate of shallow seismicity[35] driven by transient dynamic topography due to underlying mantle flow[34]. Although differential surface loading of sediment volumes likely results in localised spatially variable subsidence rates[60], geomorphological evidence from the central Sunda Shelf at Belitung Island and in the Singapore Strait (Fig. 1) indicates long-wavelength subsidence at rates of 0.2–0.3 mm/yr[34,64] that are representative for the central Sunda Shelf during the Quaternary[34].

The Quaternary stratigraphy of Singapore provides evidence of paleoenvironmental change from intertidal sediments and sea-level indicators preserved in paleo channels, coastal deposits and deep-drill boreholes[64,73,74,83,85]. The natural predeveloped coastline of Singapore was encompassed by extensive coastal to shallow marine ecosystems including coral reefs, intertidal flats, and mangrove forests[100–102,122]. Rapid industrial and urban development during the 20th century, however, has since reduced habitat extent to relatively small remnant patches mainly positioned along northern coastlines and offshore islands (Fig. 1b). The coastal waters surrounding Singapore and in the Johor Strait are relatively shallow (<20 m) but reach depths of ~30 m to ~120 m in the Singapore Strait[64,92] (Fig. 1b). Today, water flow through the region connects to the Pacific Ocean via the South China Sea to the northeast, the Indian Ocean through the Malacca Strait to the west and the Java Sea to the southeast (Fig. 1a). The convergence of tidal waters within the Singapore Strait creates a diurnal and semi-diurnal tidal regime with a mean amplitude of 2.4 m during spring tides and 1 m during neap tides[8].

We compiled existing RSL data from the central Sunda Shelf, Singapore and Mapur Island, Indonesia[123] (Fig. 1a, b). The geological reconstructions and instrumental records for the Holocene, including the 20th and 21st century, use RSL data from Singapore[31] and Mapur Island, Indonesia[32], respectively. Mapur Island has minimal differences in present-day rate of GIA (<0.1 mm/yr) and sea-surface height (<2 cm) with Singapore[32]. To extend the temporal scale of the RSL reconstruction to the LGM, we included RSL data from the central Sunda Shelf[26,30]. To account for the GIA difference between the central Sunda Shelf and Singapore, we included a vertical uncertainty for the central Sunda Shelf RSL data using predictions from the ICE-6G_C global ice history model[37,38] and HetM-LHL140 3D Earth model[124,125].

The geological RSL reconstructions are based on mangrove root remnants and intertidal deposits[26,30,31] and coral microatolls[32] that are used as proxy sea-level indicators to develop SLIPs. A SLIP defines the past position of RSL in time and space with an associated vertical and temporal uncertainty[13,126]. Standardised protocols in the collation and validation of SLIP data[75] require four key attributes including: (1) elevation of the sample relative to a modern tidal datum; (2) vertical relationship of the sample to contemporaneous sea level, termed the indicative meaning; (3) age of formation or growth (e.g., through radiometric methods); and (4) geographic location.

The elevation of SLIPs on the central Sunda Shelf was measured using depths below modern water surface[26,30] and in Singapore and Mapur Island using total station surveys[31,32]. The indicative meaning of SLIPs incorporates the central tendency (reference water level) and indicative (vertical) range of the sample's distribution relative to tidal levels[126]. Indicative meanings for mangrove and coral microatoll SLIPs were established using the indicative range of modern analogues detailed in original publications[31,32]. For the Sunda Shelf SLIPs, we applied the same indicative range as those applied to SLIPs in Singapore. The age of mangrove and intertidal SLIPs were radiocarbon dated and (re)calibrated using IntCal20[127]. The age of coral microatoll SLIPs were constrained through annual growth-band counting from the living edge of the coral structure[32]. Geographic locations were extracted from original publications, respectively.

The instrumental RSL records are based on Singapore's network of tide gauge stations (Fig. 1b) that provide water level measurements during the 20th and 21st centuries of varying time length and completeness (Table 1). From these we constructed an averaged instrumental record using annual data from the four longest, most complete tide gauges including Sultan Shoal, Raffles Lighthouse, Tanjong Pagar and Sembawang (Table 1). While Sembawang was operational since 1954 CE, we excluded measurements prior to 1972 CE because of anomalously high data points that precedes a long data gap between 1961 and 1971 CE after which the station was relocated[92]. Data for Sultan Shoal are also not available prior to 1972 CE (Table 1).

Statistical analyses. We combined the geological reconstructions and averaged instrumental record and quantified magnitudes and rates of RSL change using an Error-In-Variables Integrated Gaussian Process (EIV-IGP) model[36]. The EIV-IGP model takes an unevenly distributed RSL time series, prone to vertical and temporal uncertainties, as input and produces estimates of RSL and rates of RSL with 95% credible intervals. The EIV-IGP model models rates of RSL change using a Gaussian process[128] (GP) and models RSL as the integral of the GP (IGP) plus (measured and estimated) vertical uncertainty. Temporal uncertainties are accounted for through setting the IGP model in an errors-in-variables (EIV) framework[129]. The geological reconstructions spanning the end of the LGM through the LDT and Holocene were analysed at 250-year time intervals. The combined geological and averaged instrumental record for the 20th and 21st century were analysed at annual time intervals. We included a vertical uncertainty for the averaged tide gauge record calculated from the standard deviation of RSL values following ref. [36].

We make use of the probabilistic nature of the model-based estimates from the EIV-IGP model to provide perspective to future scenario-based sea-level projections demonstrating the probability of when equivalent rates of RSL rise were last exceeded. Specifically, we use the posterior samples of RSL rise obtained from the EIV-IGP model to estimate the probability that RSL rise in a given year t exceeded sea level projections under various climate scenarios. To estimate the probabilities, we let $\omega_x^{(s)}$ be posterior sample s of RSL rise in year x and let p_x be the probability that RSL rise in year x was greater than a chosen rate of change (denoted δ), such that:

$$p_x = (1/\mathrm{M}) \sum_{s=1}^{M} \mathbb{I}(\omega_x^{(s)} > \delta) \quad (1)$$

where $\mathbb{I}$ is an indicator function such that $\mathbb{I}(\text{condition}) = 1$ if the condition in the brackets holds true and 0 otherwise. For the purposes of this study, we included values of δ reflecting projected rates of RSL rise by 2150 under different climate scenarios outlined below.

Sea-level projections. We utilise the latest, most up to date regional sea-level projection data currently available for Singapore developed by the IPCC AR6 report[4,39]. The sea-level projections adopt differing future SSP scenarios, which reflect a range of possible changes in socioeconomic conditions and the geophysical driving mechanisms of climate change, including radiative forcing and greenhouse gas emission and concentration futures[4,130]. From these SSPs, we selected sea-level rise projections to 2150 (relative to a 1995–2014 baseline period) for Singapore under SSP1-1.9, SSP2-4.5, and SSP5-8.5 emissions scenarios that broadly encompass the lowest and highest emission scenarios, respectively[4,39].

Each SSP scenario encompasses an associated GMST and greenhouse gas emission range. Under a very strong mitigation scenario (SSP1-1.9), the GMST (relative to a 1850–1900 baseline period) increase is limited to 1.0–1.8 °C warming by 2100, with net zero CO_2 emissions achieved by 2050. Under the moderate emissions scenario SSP2-4.5, GMST is limited to 2.1–3.5 °C warming by 2100, with CO_2 emissions falling by 2050 but not reaching net-zero until after 2100. Conversely, under a very high emissions scenario (SSP5-8.5) that reverses current climate policy, GMST increases 3.3–5.7 °C by 2100, with CO_2 emissions double current levels by 2050 and continuing to increase thereafter. AR6 also assessed the potential contributions to sea-level rise under SSP1-2.6 and SSP5-8.5 of ice-sheet processes, such as MICI, currently characterised by *low confidence*. We also include *low confidence* SSP5-8.5 projections as an indicator of potential high-end sea level projections. Under each SSP, we also report the projected timing of exceedance of 0.5 m and 1.0 m RSL rise magnitude thresholds.

Paleotopographic maps. We produced paleotopographic maps of the Sunda Shelf region at 500-year time intervals to demonstrate spatial and temporal land area changes and lateral shoreline migration in response to RSL change following the LGM. The maps were generated following ref. [131] and use the ICE-6G_C global ice history model[37,38] and HetM-LHL140 3D Earth model[124,125]:

$$T(\theta, \lambda, t) = S(\theta, \lambda, t) + \left[T_p(\theta, \lambda) - S\left(\theta, \lambda, t_p\right)\right] \quad (2)$$

Where, θ, λ and t represent latitude, longitude and time, respectively; $T(\theta, \lambda, t)$ is the paleotopography at time t; $T_p(\theta, \lambda)$ is the present topography from

ETOPO1[132], $S(\theta, \lambda, t_p)$ and $S(\theta, \lambda, t)$ are the present-day sea level and sea level at time t respectively, which are predicted by a GIA model with the ICE-6G_C ice history model[37,38] and the HetM-LHL140 3D earth model[124,125]. The HetM-LHL140 3D Earth model includes lateral variations both in the lithospheric thickness and mantle viscosity.

We then used the paleotopographic maps to calculate land area difference compared to the present-day topography and rates of landward lateral shoreline migration across a hypothetical transect extending from the South China Sea toward Singapore (Fig. 4a). While lateral shoreline migration rates may respond to variety of regional and local sedimentary processes, for example, delta progradation, sedimentation and erosion[133], our modelled results provide an estimated response of the paleogeographic landscape to rising RSL since the LGM.

We also compare and discuss output from the EIV-IGP model results and RSL datasets from the Sunda Shelf, Vietnam Shelf and Singapore with ICE-6G_C model predictions of RSL change (Supplementary discussion).

Data availability

The relative sea-level datasets from the geological reconstructions and instrumental records are available from the Nanyang Technological University data repository at https://doi.org/10.21979/N9/LI3E6F. The instrumental sea-level data for Singapore tide gauge stations were downloaded from https://www.psmsl.org/data/obtaining/. The ICE-6G_C ice model data profiles are available from https://www.atmosp.physics.utoronto.ca/~peltier/data.php and present-day topography data from ETOPO1 are available from https://www.ngdc.noaa.gov/mgg/global/. The sea-level projections developed by the IPCC AR6 report are available from https://sealevel.nasa.gov/ipcc-ar6-sea-level-projection-tool and raw data files available from https://doi.org/10.5281/zenodo.5914709.

Code availability

The Error-In-Variables Integrated Gaussian Process model is available from https://github.com/ncahill89/EIV_IGP.

Received: 31 October 2022; Accepted: 26 May 2023;
Published online: 08 June 2023

References

1. Kulp, S. A. & Strauss, B. H. New elevation data triple estimates of global vulnerability to sea-level rise and coastal flooding. *Nat. Commun.* **10**, 4844 (2019).
2. Nicholls, R. J. et al. A global analysis of subsidence, relative sea-level change and coastal flood exposure. *Nat. Clim. Chang.* **11**, 338–342 (2021).
3. Strauss, B. H., Kulp, S. A., Rasmussen, D. J. & Levermann, A. Unprecedented threats to cities from multi-century sea level rise. *Environ. Res. Lett.* **16**, 114015 (2021).
4. Fox-Kemper, B. et al. Ocean, Cryosphere and sea level change. in *Climate Change 2021: The Physical Science Basis. Contribution of Working Group I to the Sixth Assessment Report of the Intergovernmental Panel on Climate Change* (eds. Masson-Delmotte, V. et al.) (Cambridge University Press, 2021).
5. Tay, C. et al. Sea-level rise from land subsidence in major coastal cities. *Nat. Sustain.* **5**, 1049–1057 (2022).
6. Kirezci, E. et al. Projections of global-scale extreme sea levels and resulting episodic coastal flooding over the 21st Century. *Sci. Rep.* **10**, 11629 (2020).
7. Hooijer, A. & Vernimmen, R. Global LiDAR land elevation data reveal greatest sea-level rise vulnerability in the tropics. *Nat. Commun.* **12**, 3592 (2021).
8. Wong, P. P. Impact of a sea level rise on the coasts of Singapore: preliminary observations. *J. Southeast Asian Earth Sci.* **7**, 65–70 (1992).
9. Cannaby, H. et al. Projected sea level rise and changes in extreme storm surge and wave events during the 21st century in the region of Singapore. *Ocean Sci.* **12**, 613–632 (2016).
10. Ng, W.-S. & Mendelsohn, R. The impact of sea level rise on Singapore. *Environ. Dev. Econ.* **10**, 201–215 (2005).
11. Milne, G. A., Gehrels, W. R., Hughes, C. W. & Tamisiea, M. E. Identifying the causes of sea-level change. *Nat. Geosci.* **2**, 471–478 (2009).
12. Clark, P. U. et al. Consequences of twenty-first-century policy for multi-millennial climate and sea-level change. *Nat. Clim. Change* **6**, 360–369 (2016).
13. Horton, B. P. et al. Mapping sea-level change in time, space, and probability. *Annu. Rev. Environ. Resourc.* **43**, 481–521 (2018).
14. Church, J. A. & White, N. J. Sea-level rise from the late 19th to the early 21st century. *Surv. Geophys.* **32**, 585–602 (2011).
15. Holgate, S. J. et al. New data systems and products at the permanent service for mean sea level. *J. Coast. Res.* **15**, 493–504 (2013).
16. Kemp, A. C. et al. Climate related sea-level variations over the past two millennia. *Proc. Natl Acad. Sci.* **108**, 11017–11022 (2011).
17. Kopp, R. E. et al. Temperature-driven global sea-level variability in the Common Era. *Proc. Natl Acad. Sci.* **113**, E1434–E1441 (2016).
18. Miller, K. G., Kopp, R. E., Horton, B. P., Browning, J. V. & Kemp, A. C. A geological perspective on sea-level rise and its impacts along the U.S. mid-Atlantic coast. *Earth's Future* **1**, 3–18 (2013).
19. Lambeck, K., Rouby, H., Purcell, A., Sun, Y. & Sambridge, M. Sea level and global ice volumes from the Last Glacial Maximum to the Holocene. *Proc. Natl Acad. Sci.* **111**, 15296–15303 (2014).
20. Kemp, A. C., Dutton, A. & Raymo, M. E. Paleo constraints on future sea-level rise. *Curr. Clim. Change. Rep.* **1**, 205–215 (2015).
21. Kopp, R. E., Hay, C. C., Little, C. M. & Mitrovica, J. X. Geographic variability of sea-level change. *Curr Clim Change Rep.* **1**, 192–204 (2015).
22. Khan, N. S. et al. Holocene relative sea-level changes from near-, intermediate-, and far-field locations. *Curr. Clim. Change Rep.* **1**, 247–262 (2015).
23. Yokoyama, Y. & Purcell, A. On the geophysical processes impacting palaeo-sea-level observations. *Geosci. Lett.* **8**, 13 (2021).
24. Fairbanks, R. G. A 17,000-year glacio-eustatic sea level record: influence of glacial melting rates on the Younger Dryas event and deep-ocean circulation. *Nature* **342**, 637–642 (1989).
25. Bard, E. et al. Deglacial sea-level record from Tahiti corals and the timing of global meltwater discharge. *Nature* **382**, 241–244 (1996).
26. Hanebuth, T., Stattegger, K. & Grootes, P. M. Rapid flooding of the sunda shelf: a late-glacial sea-level record. *Science* **288**, 1033–1035 (2000).
27. Yokoyama, Y., Lambeck, K., De Deckker, P., Johnston, P. & Fifield, L. K. Timing of the Last Glacial Maximum from observed sea-level minima. *Nature* **406**, 713–716 (2000).
28. Peltier, W. R. & Fairbanks, R. G. Global glacial ice volume and Last Glacial Maximum duration from an extended Barbados sea level record. *Quat. Sci. Re.* **25**, 3322–3337 (2006).
29. Palmer, M. D. et al. Exploring the drivers of global and local sea-level change over the 21st century and beyond. *Earth's Future* **8**, e2019EF001413 (2020).
30. Hanebuth, T. J. J., Stattegger, K. & Bojanowski, A. Termination of the Last Glacial Maximum sea-level lowstand: the Sunda-Shelf data revisited. *Glob. Planet. Change* **66**, 76–84 (2009).
31. Chua, S. et al. A new Holocene sea-level record for Singapore: *The Holocene.* **31**, 1376–1390 (2021).
32. Majewski, J. M. et al. Extending instrumental sea-level records using coral microatolls, an example from Southeast Asia. *Geophys. Res. Lett.* **49**, e2021GL095710 (2022).
33. Tjia, H. D. Sea-level changes in the tectonically stable Malay-Thai Peninsula. *Quat. Int.* **31**, 95–101 (1996).
34. Sarr, A.-C. et al. Subsiding Sundaland. *Geology* **47**, 119–122 (2019).
35. Simons, W. J. F. et al. A decade of GPS in Southeast Asia: resolving Sundaland motion and boundaries. *J. Geophys. Res. Solid Earth* **112**, B06420 (2007).
36. Cahill, N., Kemp, A. C., Horton, B. P. & Parnell, A. C. Modeling sea-level change using errors-in-variables integrated Gaussian processes. *Ann. Appl. Stat.* **9**, 547–571 (2015).
37. Peltier, W. R., Argus, D. F. & Drummond, R. Space geodesy constrains ice age terminal deglaciation: The global ICE-6G_C (VM5a) model. *J. Geophys. Res. Solid Earth* **120**, 2014JB011176 (2015).
38. Argus, D. F., Peltier, W. R., Drummond, R. & Moore, A. W. The Antarctica component of postglacial rebound model ICE-6G_C (VM5a) based on GPS positioning, exposure age dating of ice thicknesses, and relative sea level histories. *Geophys. J. Int.* **198**, 537–563 (2014).
39. Garner, G. et al. IPCC AR6 sea-level rise projections. Version 20210809. PO.DAAC, CA, USA. https://podaac.jpl.nasa.gov/announcements/2021-08-09-Sea-level-projections-from-the-IPCC-6th-Assessment-Report. (2021).
40. Clark, P. U. et al. The Last Glacial Maximum. *Science* **325**, 710–714 (2009).
41. Osman, M. B. et al. Globally resolved surface temperatures since the Last Glacial Maximum. *Nature* **599**, 239–244 (2021).
42. Gulev, S. K. et al. Changing state of the climate system. In: *Climate Change 2021: The Physical Science Basis. Contribution of Working Group I to the Sixth Assessment Report of the Intergovernmental Panel on Climate Change*. (eds. Masson-Delmotte, V. et al.) (Cambridge University Press, 2021).
43. He, F. et al. Northern Hemisphere forcing of Southern Hemisphere climate during the last deglaciation. *Nature* **494**, 81–85 (2013).
44. Lambeck, K., Esat, T. M. & Potter, E.-K. Links between climate and sea levels for the past three million years. *Nature* **419**, 199–206 (2002).
45. Peltier, W. R. On eustatic sea level history: last Glacial Maximum to Holocene. *Quat. Sci. Rev.* **21**, 377–396 (2002).
46. Carlson, A. E. & Clark, P. U. Ice sheet sources of sea level rise and freshwater discharge during the last deglaciation. *Rev. Geophys.* **50**, RG4007 (2012).

47. Harrison, S., Smith, D. E. & Glasser, N. F. Late Quaternary meltwater pulses and sea level change. *J. Quat. Sci.* **34**, 1–15 (2019).
48. Clark, C. D. et al. Map and GIS database of glacial landforms and features related to the last British Ice Sheet. *Boreas* **33**, 359–375 (2004).
49. Deschamps, P. et al. Ice-sheet collapse and sea-level rise at the Bølling warming 14,600 years ago. *Nature* **483**, 559–564 (2012).
50. Peltier, W. R. On the hemispheric origins of meltwater pulse 1a. *Quat. Sci. Rev.* **24**, 1655–1671 (2005).
51. Lin, Y. et al. A reconciled solution of Meltwater Pulse 1A sources using sea-level fingerprinting. *Nat. Commun.* **12**, 2015 (2021).
52. Shennan, I., Hamilton, S., Hillier, C. & Woodroffe, S. A 16000-year record of near-field relative sea-level changes, northwest Scotland, United Kingdom. *Quat. Int.* **133–134**, 95–106 (2005).
53. Liu, J. P. & Milliman, J. D. Reconsidering melt-water pulses 1A and 1B: global impacts of rapid sea-level rise. *J. Ocean Univ. China* **3**, 183–190 (2004).
54. Abdul, N. A., Mortlock, R. A., Wright, J. D. & Fairbanks, R. G. Younger Dryas sea level and meltwater pulse 1B recorded in Barbados reef crest coral Acropora palmata. *Paleoceanography* **31**, 330–344 (2016).
55. Gargani, J. Relative sea level and abrupt mass unloading in Barbados during the Holocene. *Geomorphology* **413**, 108353 (2022).
56. Tjallingii, R., Stattegger, K., Stocchi, P., Saito, Y. & Wetzel, A. Rapid flooding of the southern Vietnam shelf during the early to mid-Holocene. *J. Quat. Sci.* **29**, 581–588 (2014).
57. De Groeve, J. et al. Global raster dataset on historical coastline positions and shelf sea extents since the Last Glacial Maximum. *Glob. Ecol. Biogeogr.* **31**, 2162–2171 (2022).
58. Hanebuth, T. J. J. & Stattegger, K. The stratigraphic evolution of the Sunda shelf during the past fifty thousand years. In: *Tropical Deltas of Southeast Asia —Sedimentology, Stratigraphy, and Petroleum Geology* (eds. Sidi, F. H., Nummedal, D., Imbert, P., Darman, H. & Posamentier, H. W.) vol. 76 0 (SEPM Society for Sedimentary Geology, 2003).
59. Bird, M. I., Taylor, D. & Hunt, C. Palaeoenvironments of insular Southeast Asia during the Last Glacial Period: a Savanna corridor in Sundaland? *Quat. Sci. Rev.* **24**, 2228–2242 (2005).
60. Hanebuth, T. J. J., Voris, H. K., Yokoyama, Y., Saito, Y. & Okuno, J. Formation and fate of sedimentary depocentres on Southeast Asia's Sunda Shelf over the past sea-level cycle and biogeographic implications. *Earth-Sci. Rev.* **104**, 92–110 (2011).
61. Wang, X., Sun, X., Wang, P. & Stattegger, K. Vegetation on the Sunda Shelf, South China Sea, during the Last Glacial Maximum. *Palaeogeogr., Palaeoclimatol., Palaeoecol.* **278**, 88–97 (2009).
62. Sun, X., Li, X., Luo, Y. & Chen, X. The vegetation and climate at the last glaciation on the emerged continental shelf of the South China Sea. *Palaeogeogr., Palaeoclimatol., Palaeoecol.* **160**, 301–316 (2000).
63. Kim, H. L. et al. Prehistoric human migration between Sundaland and South Asia was driven by sea-level rise. *Commun. Biol.* **6**, 150 (2023).
64. Bird, M. I., Pang, W. C. & Lambeck, K. The age and origin of the Straits of Singapore. *Palaeogeogr. Palaeoclimatol. Palaeoecol.* **241**, 531–538 (2006).
65. Wang, L. et al. East Asian monsoon climate during the Late Pleistocene: high-resolution sediment records from the South China Sea. *Mar. Geol.* **156**, 245–284 (1999).
66. Griffiths, M. L. et al. Increasing Australian–Indonesian monsoon rainfall linked to early Holocene sea-level rise. *Nat. Geosci.* **2**, 636–639 (2009).
67. Liu, G. et al. On the glacial-interglacial variability of the Asian monsoon in speleothem δ18O records. *Sci. Adv.* **6**, eaay8189 (2020).
68. Rehfeld, K., Münch, T., Ho, S. L. & Laepple, T. Global patterns of declining temperature variability from the Last Glacial Maximum to the Holocene. *Nature* **554**, 356–359 (2018).
69. Bova, S., Rosenthal, Y., Liu, Z., Godad, S. P. & Yan, M. Seasonal origin of the thermal maxima at the Holocene and the last interglacial. *Nature* **589**, 548–553 (2021).
70. Smith, D. E., Harrison, S., Firth, C. R. & Jordan, J. T. The early Holocene sea level rise. *Quat. Sci. Rev.* **30**, 1846–1860 (2011).
71. Stroeven, A. P. et al. Deglaciation of Fennoscandia. *Quat. Sci. Rev.* **147**, 91–121 (2016).
72. Ullman, D. J. et al. Final Laurentide ice-sheet deglaciation and Holocene climate-sea level change. *Quat. Sci. Rev.* **152**, 49–59 (2016).
73. Bird, M. I. et al. An inflection in the rate of early mid-Holocene eustatic sea-level rise: a new sea-level curve from Singapore. *Estuar. Coast. Shelf Sci.* **71**, 523–536 (2007).
74. Bird, M. I. et al. Punctuated eustatic sea-level rise in the early mid-Holocene. *Geology* **38**, 803–806 (2010).
75. Khan, N. S. et al. Inception of a global atlas of sea levels since the Last Glacial Maximum. *Quat. Sci. Rev.* **220**, 359–371 (2019).
76. Horton, B. P. et al. Holocene sea levels and palaeoenvironments, Malay-Thai Peninsula, southeast Asia. *Holocene* **15**, 1199–1213 (2005).
77. Mann, T. et al. Holocene sea levels in Southeast Asia, Maldives, India and Sri Lanka: the SEAMIS database. *Quat. Sci. Rev.* **219**, 112–125 (2019).
78. Mitrovica, J. X. & Milne, G. A. On the origin of late Holocene sea-level highstands within equatorial ocean basins. *Quat. Sci. Rev.* **21**, 2179–2190 (2002).
79. Mitrovica, J. X., Tamisiea, M. E., Davis, J. L. & Milne, G. A. Recent mass balance of polar ice sheets inferred from patterns of global sea-level change. *Nature* **409**, 1026–1029 (2001).
80. Culver, S. J., Leorri, E., Mallinson, D. J., Corbett, D. R. & Shazili, N. A. M. Recent coastal evolution and sea-level rise, Setiu Wetland, Peninsular Malaysia. *Palaeogeogr. Palaeoclimatol. Palaeoecol.* **417**, 406–421 (2015).
81. Tam, C.-Y. et al. A below-the-present late Holocene relative sea level and the glacial isostatic adjustment during the Holocene in the Malay Peninsula. *Quat. Sci. Rev.* **201**, 206–222 (2018).
82. Zhang, Y. et al. The middle-to-late Holocene relative sea-level history, highstand and levering effect on the east coast of Malay Peninsula. *Glob. Planet. Change* **196**, 103369 (2021).
83. Hesp, P. A., Hung, C. C., Hilton, M., Ming, C. L. & Turner, I. M. A First tentative holocene sea-level curve for Singapore. *J. Coast. Res.* **14**, 308–314 (1998).
84. Saintilan, N. et al. Thresholds of mangrove survival under rapid sea level rise. *Science* **368**, 1118–1121 (2020).
85. Chua, S. et al. A new Quaternary stratigraphy of the Kallang River Basin, Singapore: Implications for urban development and geotechnical engineering in Singapore. *J. Asian Earth Sci.* **200**, 104430 (2020).
86. Climate Change 2021: *The physical science basis. Contribution of Working Group I to the Sixth Assessment Report of the Intergovernmental Panel on Climate Change*. (Cambridge University Press, 2021).
87. Keeling, C. D. et al. Exchanges of Atmospheric CO_2 and $13CO_2$ with the terrestrial biosphere and oceans from 1978 to 2000. I. Global Aspects. SIO Reference Series, No. 01-06, *UC San Diego: Scripps Institution of Oceanography, San Diego*, 88 (2001).
88. Dangendorf, S. et al. Persistent acceleration in global sea-level rise since the 1960s. *Nat. Clim. Chang.* **9**, 705–710 (2019).
89. Frederikse, T. et al. The causes of sea-level rise since 1900. *Nature* **584**, 393–397 (2020).
90. Palmer, M. D., Domingues, C. M., Slangen, A. B. A. & Dias, F. B. An ensemble approach to quantify global mean sea-level rise over the 20th century from tide gauge reconstructions. *Environ. Res. Lett.* **16**, 044043 (2021).
91. Walker, J. S., Kopp, R. E., Little, C. M. & Horton, B. P. Timing of emergence of modern rates of sea-level rise by 1863. *Nat. Commun.* **13**, 1–8 (2022).
92. Tkalich, P., Vethamony, P., Luu, Q.-H. & Babu, M. T. Sea level trend and variability in the Singapore Strait. *Ocean Sci.* **9**, 293–300 (2013).
93. Luu, Q. H., Tkalich, P. & Tay, T. W. Sea level trend and variability around Peninsular Malaysia. *Ocean Sci.* **11**, 617–628 (2015).
94. Fu, Y., Zhou, X., Zhou, D., Li, J. & Zhang, W. Estimation of sea level variability in the South China Sea from satellite altimetry and tide gauge data. *Adv. Space Res.* **68**, 523–533 (2021).
95. Qu, Y., Jevrejeva, S., Williams, J. & Moore, J. C. Drivers for seasonal variability in sea level around the China seas. *Glob. Planet. Change.* **213**, 103819 (2022).
96. Tkalich, P., Vethamony, P., Babu, M. T. & Malanotte-Rizzoli, P. Storm surges in the Singapore Strait due to winds in the South China Sea. *Nat Hazards* **66**, 1345–1362 (2013).
97. Hamlington, B. D. et al. The dominant global modes of recent internal sea level variability. *J. Geophys. Res. Oceans* **124**, 2750–2768 (2019).
98. Han, W. et al. Spatial patterns of sea level variability associated with natural internal climate modes. *Surv Geophys* **38**, 217–250 (2017).
99. Powell, M. A. Singapore's lost coast: land reclamation, national development and the erasure of human and ecological communities, 1822-present. *Environ. History* **27**, 635–663 (2021).
100. Corlett, R. T. The ecological transformation of Singapore, 1819-1990. *J. Biogeogr.* **19**, 411–420 (1992).
101. Hilton, M. J. & Manning, S. S. Conversion of coastal habitats in Singapore: indications of unsustainable development. *Environ. Conserv.* **22**, 307–322 (1995).
102. Lai, S., Loke, L. H. L., Hilton, M. J., Bouma, T. J. & Todd, P. A. The effects of urbanisation on coastal habitats and the potential for ecological engineering: a Singapore case study. *Ocean Coast. Manag.* **103**, 78–85 (2015).
103. Gowan, E. J. et al. A new global ice sheet reconstruction for the past 80 000 years. *Nat. Commun.* **12**, 1–9 (2021).
104. Levermann, A. et al. The multimillennial sea-level commitment of global warming. *Proc. Natl Acad. Sci.* **110**, 13745–13750 (2013).
105. Clark, P. U. et al. Sea-level commitment as a gauge for climate policy. *Nat. Clim Change* **8**, 653–655 (2018).
106. Mengel, M., Nauels, A., Rogelj, J. & Schleussner, C.-F. Committed sea-level rise under the Paris Agreement and the legacy of delayed mitigation action. *Nat. Commun.* **9**, 1–10 (2018).
107. Nauels, A. et al. Attributing long-term sea-level rise to Paris Agreement emission pledges. *Proc. Natl Acad. Sci.* **116**, 23487–23492 (2019).

108. Dutton, A. et al. Sea-level rise due to polar ice-sheet mass loss during past warm periods. *Science* **349**, aaa4019 (2015).
109. Kopp, R. E., Simons, F. J., Mitrovica, J. X., Maloof, A. C. & Oppenheimer, M. Probabilistic assessment of sea level during the last interglacial stage. *Nature* **462**, 863–867 (2009).
110. Dyer, B. et al. Sea-level trends across The Bahamas constrain peak last interglacial ice melt. *Proc. Natl Acad. Sci.* **118**, e2026839118 (2021).
111. DeConto, R. M. & Pollard, D. Contribution of Antarctica to past and future sea-level rise. *Nature* **531**, 591–597 (2016).
112. DeConto, R. M. et al. The Paris Climate Agreement and future sea-level rise from Antarctica. *Nature* **593**, 83–89 (2021).
113. Molengraaff, G. A. F. & Weber, M. On the relation between the pleistocene glacial period and the origin of the Sunda sea (Java and South China-sea), and its influence on the distribution of coralreefs and on the land- and freshwater fauna. *Proc. R. Acad.* **23**, 395–439 (1921).
114. Dickerson, R. E. Molengraaff river; a drowned Pleistocene stream and other Asian evidences bearing upon the lowering of sea level during the ice age. in *Shiftings of Sea Floors and Coast Lines* (eds. Bowen, N. L., Cushman, J. A. & Dickerson, R. E.) (University of Pennsylvania, Bicentennial Conference, 1941).
115. Voris, H. K. Maps of Pleistocene sea levels in Southeast Asia: shorelines, river systems and time durations. *J. Biogeogr.* **27**, 1153–1167 (2000).
116. Twarog, M. R. et al. Depositional environments and sequence stratigraphy of post-last glacial maximum incised valley-fill, Malay Basin, northern Sunda Shelf. *Mar. Geol.* **436**, 106457 (2021).
117. Hall, R. Sundaland and Wallacea: geology, plate tectonics and palaeogeography in *Biotic Evolution and Environmental Change in Southeast Asia* (ed Gower, D. J et al.) 32–78 (Cambridge University Press, 2012).
118. Metcalfe, I. Tectonic framework and Phanerozoic evolution of Sundaland. *Gondwana Res.* **19**, 3–21 (2011).
119. Mallick, R. et al. Long-lived shallow slow-slip events on the Sunda megathrust. *Nat. Geosci.* **14**, 327–333 (2021).
120. Whelley, P. L., Newhall, C. G. & Bradley, K. E. The frequency of explosive volcanic eruptions in Southeast Asia. *Bull. Volcanol.* **77**, 1–11 (2015).
121. Tjia, H. D. & Liew, K. K. Changes in tectonic stress field in northern Sunda Shelf basins. *Geol. Soc. Spec. Publ.* **106**, 291–306 (1996).
122. Tan, K. S., Acerbi, E. & Lauro, F. M. Marine habitats and biodiversity of Singapore's coastal waters: a review. *Reg. Stud. Mar. Sci.* **8**, 340–352 (2016).
123. Datasets for Deglacial perspectives of future sea level for Singapore. https://doi.org/10.21979/N9/LI3E6F.
124. Li, T., Wu, P., Steffen, H. & Wang, H. In search of laterally heterogeneous viscosity models of glacial isostatic adjustment with the ICE-6G_C global ice history model. *Geophys. J. Int.* **214**, 1191–1205 (2018).
125. Li, T. & Wu, P. Laterally heterogeneous lithosphere, asthenosphere and sub-lithospheric properties under Laurentia and Fennoscandia from Glacial Isostatic Adjustment. *Geophys. J. Int.* **216**, 1633–1647 (2019).
126. Shennan, I., Long, A. & Horton, B. P. *Handbook of Sea-Level Research*. (Wiley, 2015).
127. Reimer, P. et al. The IntCal20 Northern Hemisphere radiocarbon age calibration curve (0-55 cal kBP). *Radiocarbon* **62**, 725–757 (2020).
128. Williams, C. K. I. & Rasmussen, C. E. *Gaussian Processes for Regression*. (MIT Press, 1996).
129. Dey, D. K., Ghosh, S. K. & Mallick, B. K. *Generalized Linear Models: A Bayesian Perspective*. (CRC Pres, 2000).
130. O'Neill, B. C. et al. The roads ahead: Narratives for shared socioeconomic pathways describing world futures in the 21st century. *Glob. Environ. Change* **42**, 169–180 (2017).
131. Peltier, W. R. Global glacial isostasy and the surface of the ice-age earth: the ICE-5G (VM2) model and grace. *Annu. Rev. Earth Planet. Sci.* **32**, 111–149 (2004).
132. Amante, C. & Eakins, B. W. ETOPO1 Global Relief Model converted to PanMap layer format. *NOAA-National Geophysical Data Center* https://doi.org/10.1594/PANGAEA.769615 (2009).
133. Jarriel, T., Swartz, J. & Passalacqua, P. Global rates and patterns of channel migration in river deltas. *Proc. Natl Acad. Sci.* **118**, e2103178118 (2021).
134. Yokoyama, Y. et al. Rapid glaciation and a two-step sea level plunge into the Last Glacial Maximum. *Nature* **559**, 603–607 (2018).
135. Edwards, R. L. et al. A large drop in atmospheric 14 C/12 C and reduced melting in the Younger Dryas, documented with 230th ages of corals. *Science* **260**, 962–968 (1993).
136. Cutler, K. B. et al. Rapid sea-level fall and deep-ocean temperature change since the last interglacial period. *Earth Planet Sci Lett.* **206**, 253–271 (2003).

Acknowledgements

This research was supported by the Earth Observatory of Singapore grants M4430132.B50-2014, M4430139.B50-2015, M4430188.B50-2016, M4430245.B50-2017 and M4430245.B50-2018. T.A.S., T.L., S.C., J.M.M., A.D.S. and B.P.H. were supported by the Singapore Ministry of Education Academic Research Fund MOE2019-T3-1-004 and MOE-T2EP50120-0007, the National Research Foundation Singapore, the Singapore Ministry of Education under the Research Centers of Excellence initiative, and by Nanyang Technological University. This Research/Project is supported by the National Research Foundation, Singapore, and National Environment Agency, Singapore under the National Sea Level Programme Funding Initiative (award No. USS-IF-2020-1). Any opinions, findings and conclusions or recommendations expressed in this material are those of the author(s) and do not reflect the views of the National Research Foundation, Singapore and the National Environment Agency, Singapore. N.C. research is conducted with the financial support of Science Foundation Ireland and co-funded by Geological Survey Ireland under Grant number 20/FFP-P/8610. R.E.K. and G.G.G. were supported by U.S. National Science Foundation award ICER-2103754 as part of the Megalopolitan Coastal Transformation Hub (MACH) and by the National Aeronautics and Space Administration (award 80NSSC20K1724 and JPL task 105393.509496.02.08.13.31). The GIA modelling was conducted in part using the research computing facility and/or advisory services offered by the Information technology Services, the University of Hong Kong. We thank the projection authors for developing and making the sea-level rise projections available, multiple funding agencies for supporting the development of the projections, and the NASA Sea Level Change Team for developing and hosting the IPCC AR6 Sea Level Projection Tool. This publication is a contribution towards PALSEA (Palaeo-Constraints on Sea-Level Rise), a working group of the International Union for Quaternary Sciences (INQUA) and Past Global Changes (PAGES), HOLSEA (Geographic variability of Holocene sea level) and International Geoscience Program (IGCP) Project 725, "Forecasting Coastal Change". This is Earth Observatory of Singapore contribution number 526.

Author contributions

T.A.S. and B.P.H. conceptualised the research design of the study. T.A.S. led the data processing and analyses, writing of the manuscript and construction of figures. T.L provided glacial isostatic adjustment model predictions and paleotopographic land change data. N.C aided with statistical modelling and probability perspective analyses. G.G.G. and R.E.K. provided IPCC AR6 sea-level projections. T.L., T.N.G., N.C., S.C., J.M.M., Y.N., G.G.G., R.E.K., T.J.J.H., A.D.S. and B.P.H. provided feedback on the data analyses, interpretation of results and all authors commented on the text.

Competing interests

The authors declare no competing interests. A.S. is an Editorial Board Member for *Communications Earth & Environment*, but was not involved in the editorial review of, nor the decision to publish this article.

Additional information

Supplementary information The online version contains supplementary material available at https://doi.org/10.1038/s43247-023-00868-5.

Correspondence and requests for materials should be addressed to Timothy A. Shaw.

Peer review information *Communications Earth & Environment* thanks the other, anonymous, reviewer(s) for their contribution to the peer review of this work. Primary Handling Editors: HL. A peer review file is available.

Reprints and permission information is available at http://www.nature.com/reprints

Publisher's note Springer Nature remains neutral with regard to jurisdictional claims in published maps and institutional affiliations.